Stretchable Liquid Metal-Based Metal-Polymer Conductors for Fully Screen-Printed Biofuel Cells

Leni Zhong[a,b], Lixue Tang[a], Shuaijian Yang[a], Zhenting Zhao[a], Zijian Zheng[b]*, Xingyu Jiang[a]*

a. Shenzhen Key Laboratory of Smart Healthcare Engineering, Guangdong Provincial Key Laboratory of Advanced Biomaterials, Department of Biomedical Engineering, Southern University of Science and Technology, Shenzhen, Guangdong 518055, China. *E-mail: jiang@sustech.edu.cn

b. School of Fashion and Textiles, Department of Applied Biology and Chemical Technology, Research Institute for Smart Energy, Research Institute for Intelligent Wearable Systems, The Hong Kong Polytechnic University, Hung Hom, Hong Kong S.A.R., China. *E-mail: tczzheng@polyu.edu.hk

ABSTRACT: We reported a straightforward and low-cost method to fabricate stretchable biofuel cells by using liquid metal-based metal-polymer conductors. The liquid-metal-based metal-polymer conductors had a conductivity of 2.7×10^5 S/m and a stretchability larger than 200 %, giving the biofuel cell good conformability to the skin. The glucose biofuel cells (BFCs) yielded a maximum power density as 14.11 μW/cm^2 at 0.31 V with 0.2 mM glucose, while the lactate BFCs reached 31.00 μW/cm^2 at 0.51 V with 15 mM lactate. The results of 24-hour short circuit current density showed that, with enough biofuel, this patch could be used over the course of an entire day for wearable sensors.

Alongside the integration of medicine and electronics into a digital era, a large number of wearable analytical devices for healthcare are emerging.[1-8] The power supply is the heart of such wearable analytical devices, determining their longevity.[9] Currently, power supplies include energy storage devices (batteries and supercapacitors) and energy harvesting devices.[10,11] Energy harvesting devices are renewable and sustainable for long-term work, including radiofrequency (RF), photovoltaic energy harvesting, thermoelectric energy harvesting, piezoelectric energy harvesting, triboelectric energy harvesting, and biofuel cells.[12-15] However, the RF, photovoltaic, and thermoelectric energy harvesting technologies are limited by surrounding environments (extra RF transceiver, light sources, and temperature differences, respectively). The piezoelectric and triboelectric energy harvesting technologies require users to complete certain actions to convert mechanical energy into electrical energy.[16] Biofuel cells are an ideal long-term power supply for wearable analytical devices because they take advantage of natural metabolites to convert biochemical energy into electrical energy.[17,18] Theoretically, as long as the organism keeps producing metabolites that serve as fuel, the biofuel cell can continuously generate energy. If biofuel cells are applied to wearable analytical devices, it would largely prolong the lifespan of devices and expand the diversity of point-of-care testing.[19,20] Also, as the increasing demand for green energy,[21] fuels and active materials of biofuel cells are biodegradable and eco-friendly, which would not contaminate the environment and could be artificially regenerated.[22] Besides, biofuel cells have unique advantages, which can be used for biosensors, toxic detection, or drug delivery.[23]

To enhance the efficiency of power conversion, wearable biofuel cells need to be largely conformal with biological interfaces.[24,25] Researchers used nanoscale wavy gold and copper as conductors of wearable analytical devices to adapt to the deformation of biosurface.[26-30] However, the fabrication is complex, and high in cost (Table S1). Printable silver inks offer a stretchable conductor for biofuel cells to resist deformation.[31] Nevertheless, silver itself can easily cause allergic reactions in localized areas of contact and is toxic.[32] Carbon-based conductors are easy to prepare and low in cost. But their low stretchability and conductivity limit their applications.

To enhance the stretchability and conformability of the biofuel cells, we used highly stretchable, compatible, and conductive liquid metal-based metal-polymer conductors (MPC) to interconnect the biofuel cells.[33,34] The MPC can come into conformal contact with the skin, offering a stable bio-interface between the device and the skin.[35] Here, we report a strategy for fabricating skin-attachable biofuel cells with MPC to largely fit the epidermal deformation.

EXPERIMENTAL SECTION

Materials and Devices. Unless otherwise noted, all reagents were from Shanghai Aladdin Biochemical Technology Co., Ltd. The eutectic Gallium and Indium (EGaIn, 4:1, 100 g) were from Haoke Technology Inc., Beijing, China. Carboxymethyl cellulose (CMC, M.W. 250000) and hydroxypropyl chitosan (> 80%) were from Macklin Inc., China. Carbon Mediator Paste C2070424P2 was from SunChemical, U. K. SYLGARD™ 184 Silicone Elastomer, from Dow Corning, America. 1x PBS was from Solarbio, China. Glucose oxidase (G2133) and Nafion solutions were from Sigma-Aldrich, America. Lactate oxidase (LCO-301) was from Toyobo, Japan. Bilirubin oxidase was from Yuanye, China. Albumin bovine (BSA) was from West Gene Biotech. Inc.

SEM images were captured by Hitachi-SU8220 with an accelerating voltage of 5 kV. The electrochemical tests were performed by a chemical workstation (Metrohm autolab/M204). The spindle-shaped sample was loaded on a

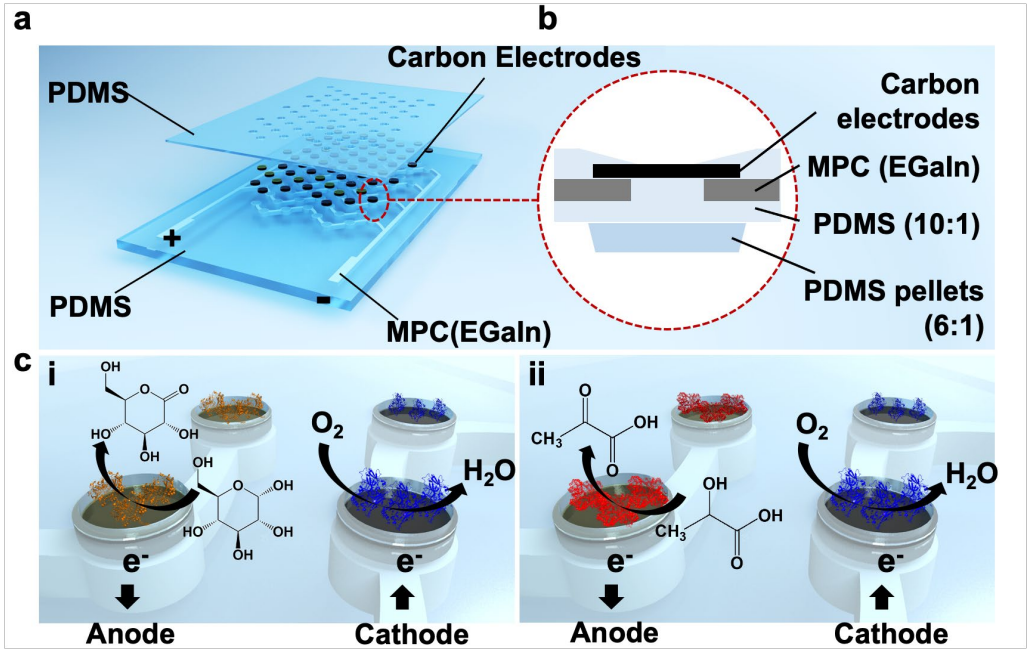

Figure 1. Scheme of a biofuel cell. (a) the structure of a biofuel cell; (b) cross-section view of the scheme of electrodes; (c) the mechanism of the biofuel cell (i: the glucose biofuel cell, ii: the lactate biofuel cell)

Universal Testing Machine (XLD-100E, Guangjing, China) with a speed of 50 mm/min. Low-power energy harvesting module (BQ25504), blood oxygen module (MAX30102), temperature module (MAX30205), and heart rate module (SON1205) were from Taobao, China.

Fabrication of MPC. To prepare EGaIn ink, we added 4 g of liquid metal and 1 mL of 1-deconal) in a 5 mL epoxy resin (EP) tube. We sonicated the mixture at 25 % amplitude with 5 s pulses and 5 s rest for a total time of 90 s by the sonicator (Sonifier SFX 20:0.55, Branson, America). Immediately, the EGaIn ink was printed on the polyethylene terephthalate (PET) film by a screen-printing method. The printed EGaIn ink was dried in an oven at 80 ℃ for 5 min. We covered a layer of PDMS on the printed EGaIn inks to fabricate MPC. After mixing PDMS and its curing agent at a ratio of 10:1, 5 ml of the mixture was added to the printed PET film and spin-coated at 200 rpm for 30 s and 400 rpm for 30 s. Then PDMS films were cured in an oven at 80 ℃. To enhance the mechanical strength and limit the strain of electrode areas, we added round pellets on the backside of the electrode areas. The round pellets were made by mixing PDMS and its curing agent at a ratio of 6:1. To increase the adhesion of the round pellets and the PDMS substrate, we used the spinning-coated method to coat another thin layer of PDMS (10:1) on the substrate (with rotating speed of 200 rpm for 30 s, 400 rpm for 15 s, and 1500 rpm for 15 s). After peeling off the PDMS substrate, the EGaIn pattern was trans-printed on the PDMS substrate (with a thickness of about 200 μm), and the MPC was formed.

Fabrication of electrodes of biofuel cells. The carbon electrode was printed by the screen-printing method with carbon paste (C2070424P2) which is designed for specific oxidase. The printed pattern was dried at 80 ℃ for 10 min. We covered a small piece of PDMS film on each carbon electrode and coated PDMS solution on other areas by spin-coating. After getting rid of the cover, the coated PDMS was cured at 60 ℃ for 2 hrs.

The carbon electrode was immersed in 0.1 M aniline and 1 M HCl solutions and connected with a three-electrode system (Ag/AgCl as the reference electrode and Pt as the counter electrode). We electrochemically polymerized a layer of polyaniline (PANI) by cyclic voltammetry from 0.2 V to 1.0 V for 25 cycles by a chemical workstation.

Fabrication of functionalized anode and cathode. We made 40 mg/mL glucose oxidase (GOD), 40 mg/mL lactate oxidase (LOx), and 10 mg/mL bilirubin oxidase (BOx) solution, respectively. The GOD or LOx was dissolved into 20 mg/mL BSA solutions (with a solvent of 1 x PBS). We dropped 2 μL of the enzymatic solution on every electrode. We dried the electrode at 4 ℃. For cathodes, we introduced 40 mM protoporphyrin IX (PPIX) solution (in 9:1 v/v ethanol/acetone) on electrodes and dried in the ambient.

Immobilization of enzymes. We used chitosan hydrogel to immobilize enzymes to prolong the life span of the BFC. We added 2 g CMC and 0.8 mL 3 M H_2SO_4 into 40 mL of deionized water. After the CMC dispersing, 20 mL $NaIO_4$ solution (with a concentration of 50 mg/mL) was added to dispersing agent at 40 ℃ water bath stirring for 4 hrs. 1.3 mL ethylene glycol was added to the dialdehyde CMC (DCMC), and kept stirring for another 0.5 hours. The solution was dialyzed in deionized water for 2 days. We obtained DCMC solid by drying the solution at 40 ℃.

We prepared 6 % hydroxypropyl chitosan solutions (300 mg in 5 mL 1 x PBS) and 6 % DCMC solutions (300 mg in 5 mL 1 x PBS). 4 parts of carboxymethyl cellulose solutions and 1 part of DCMC solutions were mixed. Before forming hydrogel, a 5 μL mixture was dropped on each bio-anode electrode.

For the biocathode, after BOx solutions dried, 2 μL 1 % Nafion (diluted with ethanol/ acetone) solution was introduced onto each biocathode. After drying the Nafion solution, the BFC was stored at 4 °C overnight to wait for the crosslinking of chitosan hydrogels.

Characterization of electrochemical performance. The electrochemical performances of the half cells and biofuel cells were conducted by the electrochemical workstation. The electrochemical characterization was performed in 0.5 M KCl solution (solved in 1x PBS solution). We used linear sweeping voltage (LSV) technology to detect the enzyme-catalyzed oxidation and oxygen reduction reactions with a sweeping rate of 10 mV/s. The three electrodes system consisted of an electrode as the working electrode, a Pt film as the counter electrode, and an Ag/AgCl (3 M KCl) as the reference electrode. The N2-saturated PBS solutions (with 0.5 M KCl) were obtained by inletting N_2 for over 30 mins.

The biofuel cell device was characterized by a two-electrode system with the bioanode as the counter and reference electrode and the biocathode as the working electrode. LSV curves of the biofuel cell in different glucose and lactate concentrations were obtained by scanning from OCP (open circuit potential) to 0.01 V at 5 mV/s. CV curves of the biofuel cell in different glucose and lactate concentrations were obtained by scanning from -0.8 to 0.7 V and from -0.4 to 0.6 V with a scanning rate of 50 mV/s. The OCP of the glucose BFC was recorded for 5 min at 0.2 mM glucose solutions (in PBS solutions with 0.5 M KCl), and the lactate BFC was recorded for 5 min at 15 mM lactate solutions.

RESULTS AND DISCUSSION

We designed a fully screen-printing stretchable biofuel cell that burns human metabolites (i.e., lactate, glucose, and so forth) to yield electrical energy (Figure 1). The biofuel cell consists of MPC, printable carbon electrodes, the stretchable polydimethylsiloxane (PDMS) substrate, and a PDMS cover (Figure 1a). We used the trans-printing method to fabricate MPC; this process is straightforward, low-cost, and can be conducted in the general environment (Figure S1). We sonicated eutectic gallium and indium (EGaIn) with decanol and printed the EGaIn ink on PET film by the screen-printing method. After drying the EGaIn ink, we cured PDMS (10:1) on top of the EGaIn ink. To enhance the strength and limit the strain of the electrode area, we added round pellets of PDMS (6:1) on the backside of the electrode (Figure 1b and Figure S2) and spin-coated another thin layer of PDMS (10:1) on the substrate to immobilize PDMS pellets. After peeling the substrate off, the EGaIn was transprinted on PDMS, and the MPC was formed. The MPC would not contact the biofuel directly. It was encapsulated by a layer of PDMS. Even the overlap of MPC and carbon ink was encapsulated by PDMS (Figure 1b). So, the MPC was stable to be conductors. SEM images showed that EGaIn particles were embedded in PDMS (Figure S3). The MPC has a conductivity of about 2.7 x 10^5 S/m, largely reducing the inner resistance of the bio-fuel cell, which is lower than that of biofuel cells made of carbon conductors. The MPC has high stretchability and deformability. The strain-stress curve of the MPC showed that the nominal tensile strain at the break of MPC was about 250 %, and the elastic deformation region was 0 % ~ 50 % of strain (Figure S4). For fuel cells, encapsulation is a critical step for maintaining usage.[33-35] EGaIn was prone to reacting with aqueous solutions, so we used carbon materials as electrodes and used PDMS to encapsulate exposed MPC. We chose commercial carbon mediator paste (C2070424P2, SunChemical) to fabricate the electrode of the biofuel cell by screen-printing methods. We used the CV method to estimate the electrochemical active surface area (ECSA) of the electrode (Figure 2a). To enhance the electrical performance of the device, we electrochemically polymerized a layer of polyaniline (PANI) by cyclic voltammetry from - 0.2 V to 1.0 V for 25 cycles (Figure 2b). The carbon electrode was immersed in 0.1 M aniline and 1 M HCl solutions and connected with a three-electrode system (Ag/AgCl as the reference electrode and Pt as the counter electrode). PANI is with multiple redox states, which show pseudocapacitance traits and contribute to the transfer of electrons from enzymes to conductors.[39] After coating, the current density of the electrode increased, which means the conductivity increased (Figure 2c). Here, PANI, with the shape of nanowire located at the top part of the carbon electrode and filled the gap of the carbon electrode. We assumed PANI increased ECSA by filling the gap of the carbon electrode, and the nanostructure contributed to the direct electron transfer from enzymes to electrodes (Figure S5).[40,41] We characterized the ECSA of the carbon electrode without and with a coating of PANI. By counting the slope of the linear fitting of the curves of current densities (at 0.0 V) against scanning rates, the double-layer capacitance per square centimeter (C_{dl}) was 0.080 μF and 0.500 μF, respectively. After being coated with PANI, the C_{dl} of the carbon electrode increased (Figure 2d).

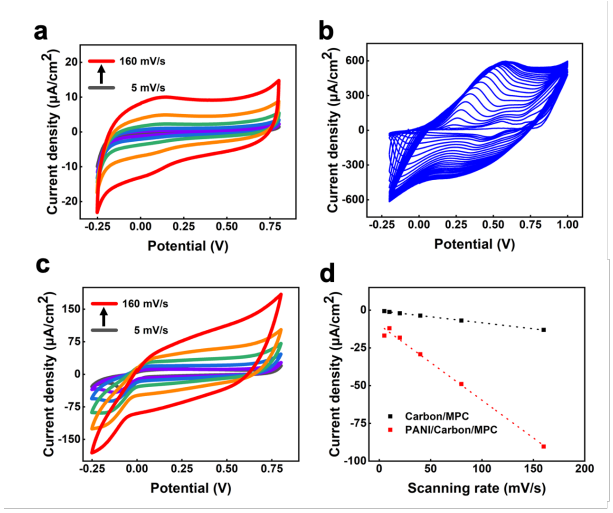

Figure 2. Electrochemical properties of electrodes of the biofuel cell. (a) CV of the carbon electrode (at 5 mV/s, 10 mV/s, 20 mV/s, 40 mV/s, 80 mV/s, 160 mV/s); (b) CV of electropolymerization of PANI; (c) CV of the carbon electrode coated with PANI (at 5 mV/s, 10 mV/s, 20 mV/s, 40 mV/s, 80 mV/s, 160 mV/s); (d) Current densities of the carbon electrode without and with PANI at 0 V against scanning rate.

To functionalize the electrode, we prepared 40 mg/mL lactate oxidase (LOx), 40 mg/mL bilirubin oxidase (BOx), and 40 mg/mL glucose oxidase (GOD), respectively. For biocathode, BOx can reduce oxygen under physiological conditions and realize direct electron transfer, so it is used as cathodic material for biosensors.[42] PPIX is the mediator of bilirubin oxidase for electron transferring, so it was added before loading BOx. PPIX has a strong π-π interaction with graphite electrodes, which can be stably adsorbed to and parallel to the graphite

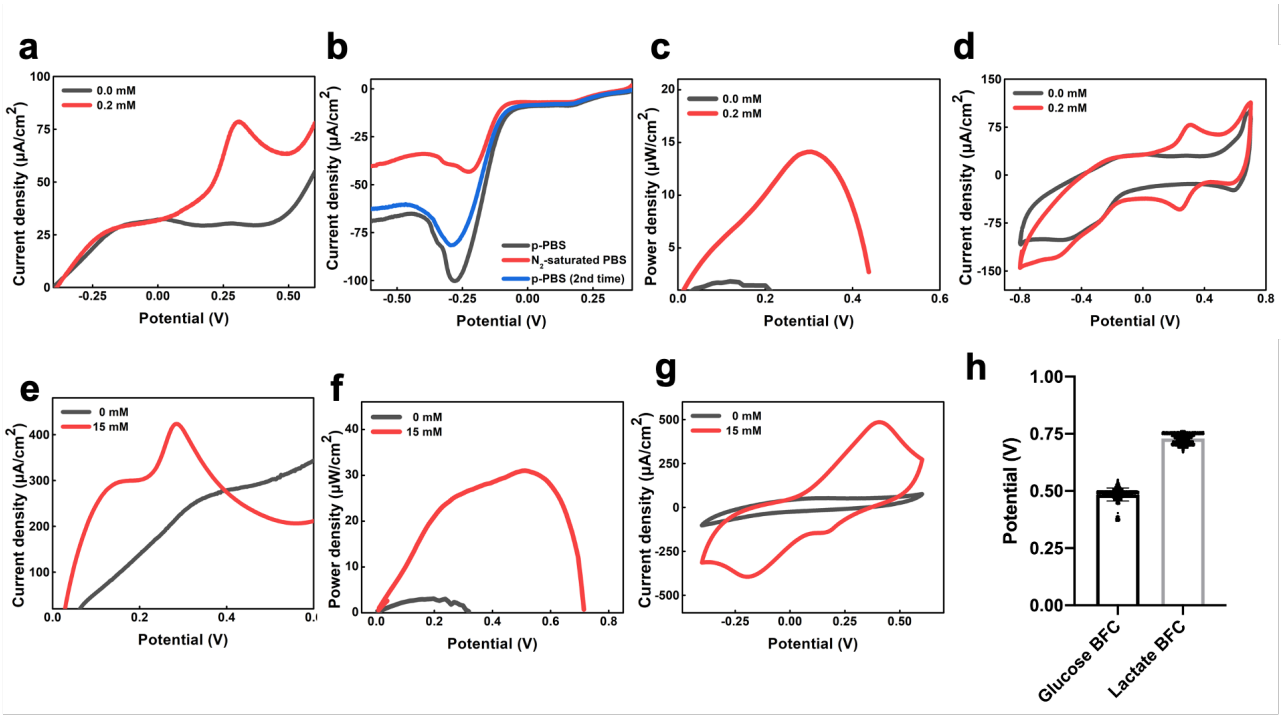

Figure 3. Electrochemical properties of the glucose and lactate biofuel cell. (a) LSV of bioanodes of glucose biofuel cells (in 0.0 mM and 0.2 mM glucose); (b) LSV of biocathode of glucose biofuel cells (in PBS, N_2 saturated PBS, and return to PBS); (c) power densities of glucose biofuel cell in 0.0 mM and 0.2 mM glucose; (d) CV of glucose biofuel cells (in 0.0 mM and 0.2 mM glucose); (e) LSV of bioanodes of lactate biofuel cells (in 0 mM and 15 mM lactate); (f) power densities of lactate biofuel cell in 0 mM and 15 mM lactate; (g) CV of lactate biofuel cells (in 0 mM and 15 mM lactate); (h) open circuit potentials of the glucose biofuel cell and the lactate biofuel cell (average in 5 min)

electrodes. The similar spatial structure of PPIX and bilirubin can affect the orientation of the BOx. The porphyrin ring parallel to the graphite electrode controls the spatial orientation of bilirubin oxidase and brings the T1 copper center of the enzyme closer to the graphite electrode, thereby enhancing the electron shuttle. For bioanodes, GOD- or LOx-modified electrodes get electrons by oxidizing glucose or lactate. The enzymes were dissolved into PBS solutions of albumin bovine (BSA). For the biofuel cell which burnt glucose, we introduced 2 μL GOD on every anode. On the whole, the glucose was catalyzed by GOD to become glucono lactone and released electrons (Figure 1ci), whereas BOx catalyzed the oxygen reduction reaction (ORR) on cathodes to catch electrons. The half-reaction mechanism of biofuel cells is shown in Formula 1 and 2.

$$Glucose \xrightarrow{GOD} e^- + Glucono\ lactone \quad (1)$$

$$O_2 + e^- \xrightarrow{BOx} H_2O \quad (2)$$

The electrochemical performances of the anode were characterized by an electrochemical workstation. We used the linear sweep voltammetry (LSV) with a scanning rate of 10 mV/s to test the polarization curves of anodes (with GOD or LOx) and cathodes. The current of electrodes with GOD increased up to the peak value of 79 μA/cm^2 at 0.31 V (vs Ag/AgCl) when the concentration of glucose increased to 0.2 mM (Figure 3a). To study the influence of O_2 on the cathodic current density, we tested the LSV of the cathode in pristine PBS solution and N_2-saturated PBS solution. As shown in Figure 3b, the current density at - 0.28 V in pristine PBS solution was near - 100.2 μA/cm^2. The current density of the reduction peak at - 0.28 V decreased dramatically. The current density at -0.28 V was increased when the cathode was tested in pristine PBS once again (p-PBS (2nd time)). The dependence of cathodic behaviour on the O_2 level indicated a normal functioning of the enzyme (Figure 3b). To characterize the electrical performance of the glucose biofuel cell, we connected the anode to the working electrode and the cathode to the referring and countering electrodes. The electrolyte was 1 x PBS solution (with 0.5 M KCl, pH~7.2). OCP of the glucose biofuel cell was 0.484 V (average in 5 min, Figure 3h). According to the LSV curve and Formula 3, when the potential reached 0.31 V, the theoretical power density was maximum (14.11 μW/cm^2).

$$P = V \times I \quad (3)$$

Where P is the power density in μW; V is the potential in V; I is the current in μA. The cyclic voltammetry (CV) curve showed that, with 0.2 mM glucose, the cell reached the maximum current density of 80 μA /cm^2 at 0.31 V. There were extra electrons transferred from the solution to the electrode (Figure 3d). We tested the LSV of the glucose biofuel cell against the concentration of glucose (0.2, 0.4, 0.8, 1.6, and 3.2 mM). The current density increased with the increase in glucose concentration (Figure S6a). When the concentration of glucose increased, the trend of the power density of glucose BFCs was increased, but the difference was mild (Figure S6b). We focused on the results with a concentration of 0.2 mM glucose, for it was close to the mean value of a healthy adult.

The strategy is also suitable for other enzymatic systems. Similarly, the lactate biofuel cell converted lactate to pyruvate

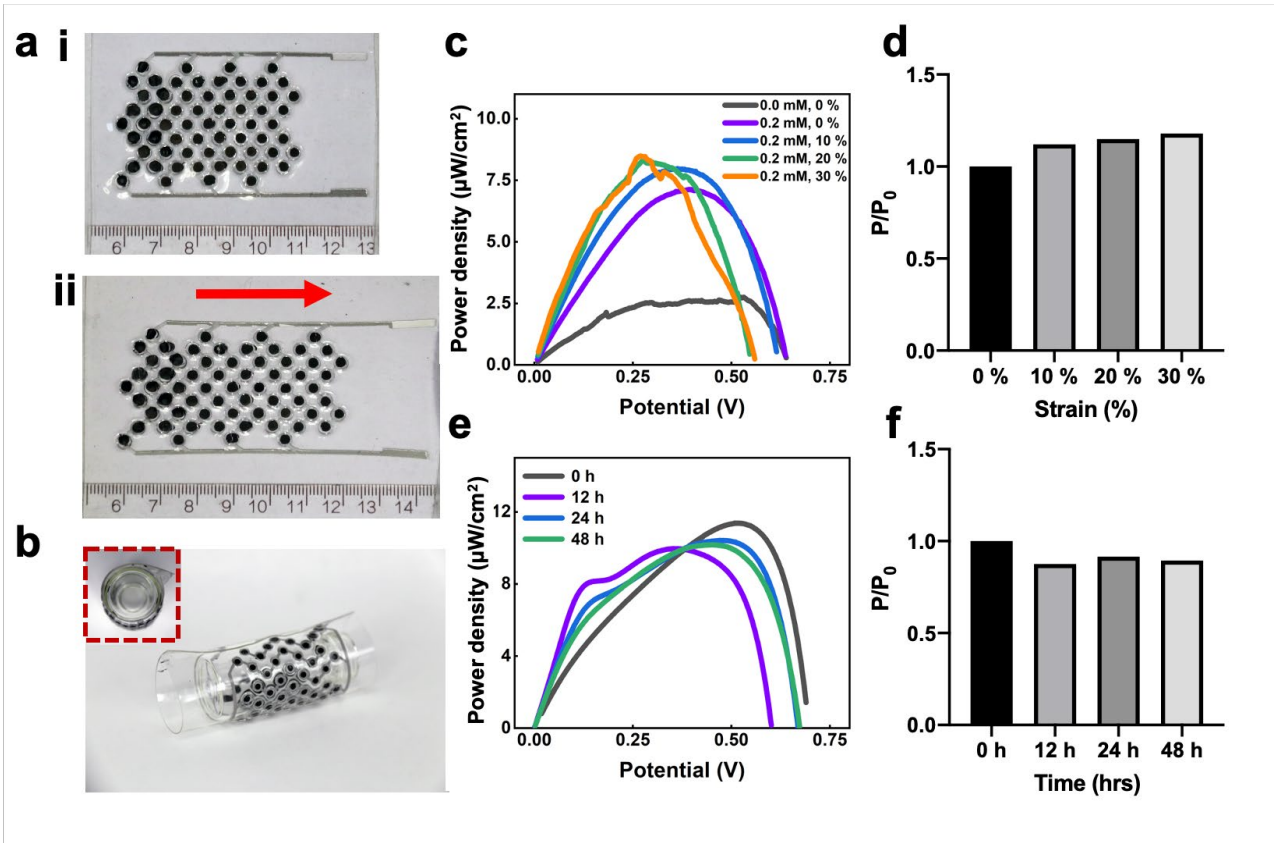

Figure 4. Strechability and stability of the BFCs. (a) the stretchability of the biofuel cell (i: the biofuel cell with a strain of 0 %, ii: the biofuel cell with a strain of 20 %); (b) Photos of the biofuel cell attaching to a curving surface; (inset: top view of the biofuel cell) (c) Power density curves of glucose BFCs with strain of 0 %, 10 %, 20 %, and 30 %; (d) the trend of power efficiency of glucose BFC with strain of 0 %, 10 %, 20 %, and 30 %. (e) Power density curves curves of glucose BFCs in 0, 12, 24, and 48 hrs; (f) the power efficiency of glucose BFC in 0, 12, 24, and 48 hrs.

(Formula 3,4 and Figure 1c ii). As proof of concept, we assembled lactate biofuel cells as well.

$$Lactate \xrightarrow{LOx} e^- + Pyruvate \quad (4)$$

$$O_2 + e^- \xrightarrow{BOx} H_2O \quad (5)$$

15 mM lactate was closer to the mean value of lactate in sweat from a healthy adult, so we focused on the results with 15 mM lactate. The characteristic result showed that, in the presence of 15 mM lactate, the main peak was located at 0.32 V (vs Ag/AgCl), and the maximum current density was up to 423.4 μA/cm^2 (Figure 3e), which meant the lactate was oxidized at this potential. The peak current density of bioanodes was positively correlated with the concentration of lactate (Figure S7a). The maximum power density of the lactate BFC was 31.00 μA/cm^2 at 0.51 V (Figure 3f). The CV result showed that with 15 mM lactate current density of the biofuel cell was larger than without one (Figure 3g). When the concentration of lactate increased, the power density of the lactate biofuel cell increased as well (Figure S7b). The lactate biofuel cell was with OCP of 0.73 V in 15 mM lactate (average in 5 min, Figure 3h).

The biofuel cell was soft, flexible, and stretchable (Figure 4a, b). In the original state of the biofuel cell, SEM images showed EGaIn particles were embedded into the PDMS, and carbon electrodes were with the structure of flakes (Figure S3c). When being stretched, the EGaIn particles were deformed along the substrate. Though the MPC had good resistance to the deformation, the carbon electrode had unsatisfactory performance in resisting deformation. With a strain of 10% lengthwise, the MPC maintained its conductivity while the carbon electrodes began to crack. To restrict the deformation of the carbon electrode, we added PDMS pellets (with a thickness of 1 mm) under the carbon electrodes (Figure S1 and Figure 1b). When the biofuel cell was with a strain of 40%, the average change of diameter of electrodes was 99.27 % ± 9.61 % ($D_{40\,\%}/D_{0\,\%}$, Table S1). There was little difference in each layer between the original state and the stretched state (Figure S4). The addition of PDMS pellets did not affect the flexibility and stretchability of the whole biofuel cell (Figure 4a, b). We studied the stretchability of the biofuel cell. When the strain began, there was a shift at maximum power density (Figure 4c). When the biofuel cell was in a strain of 30 %, the maximum power density had little increase, and the open circuit potential had a little decrease (Figure 4d). We assumed this was because of the decrease in the inner resistance of MPC. The maximum power density value with a strain of 30 % remained at 8.4 μW/cm^2. Also, we studied the stability of the biofuel cell. We tested the power density of the glucose biofuel cell with 0.2 mM glucose in the electrolyte (Figure 4e). The maximum power density was decreased when the usage time increased. After 48 hours, the power density remained at 89 %

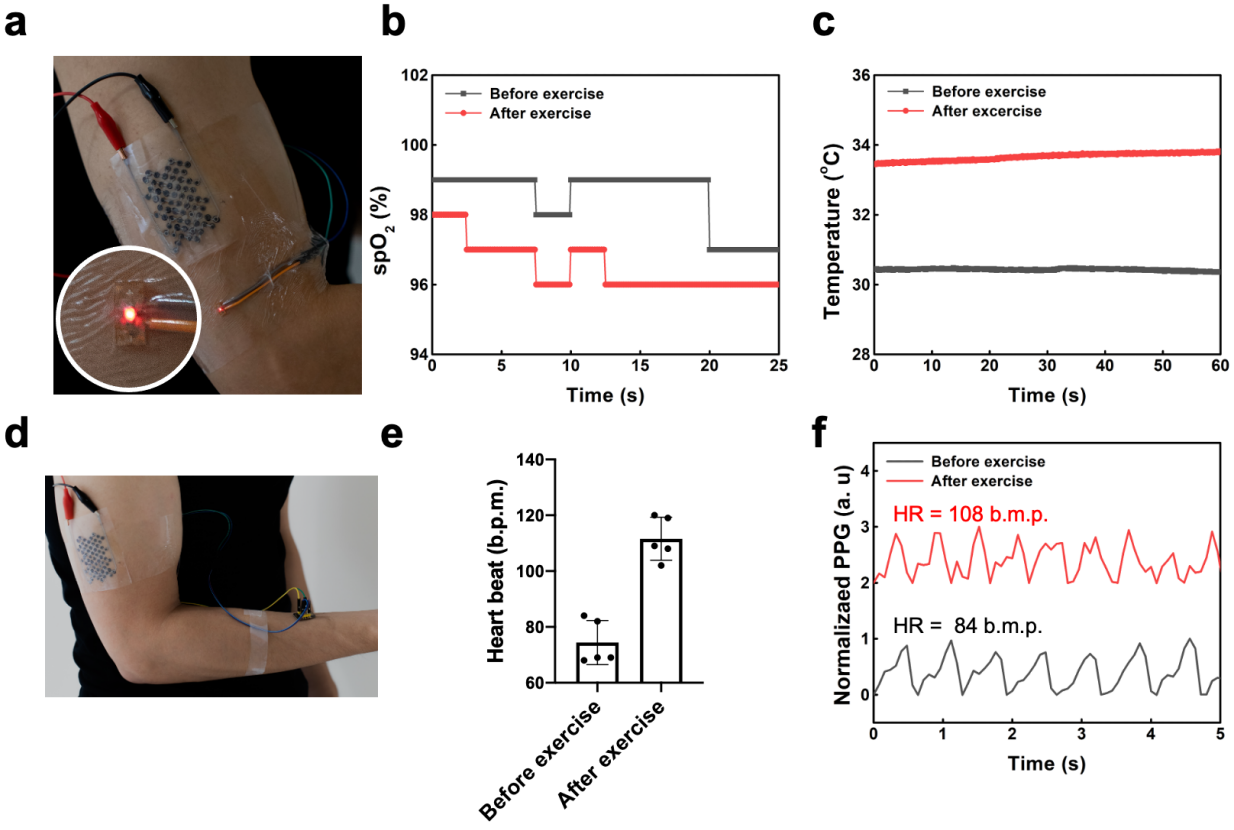

Figure 5. Application of biofuel cells. (a) red LED light lightened by biofuel cells; (b) spO_2 values of the subject before and after exercise; (c) temperature of subject before and after exercise; (d) photo of the subject wearing an oximeter module; (e) the heart rates and (f) PPG signals of tester before and after exercise.

of the original value (Figure 4f). Also, we tested the short circuit current of the lactate BFC. The testing was conducted in the static electrolyte with 32 mM lactate to offer enough substrate for catalysts (Figure S8). The result showed that the current density increased to the peak value (93 $\mu A/cm^2$) at the 12th min, then decreased to 0 at the 6th hour. The current density returned to 18 $\mu A/cm^2$ after compensating the substrate to the interface of electrodes by stirring. There was a reduction happening at the 21st hour. Twenty-one hours of durability for a patch is enough for one-day usage.

To further explore the application of biofuel cells in wearable devices, we combined it with an energy harvesting module and used it to power sensors. Considering the output voltage of the fuel cell itself is lower than the working voltage of the current wearable electronic modules (usually 3 V ~ 5 V), to enable the wearable electronic module to function, we connected a low-power energy harvesting module (Figure S8) with the biofuel cell. The electricity generated by the biofuel cell is continuously collected and stored in the energy harvesting module. For convenience, we named the whole part of the energy harvesting module and biofuel cell as the power supply module. The voltage output from the power supply module could reach 4.6V, which met the requirement of power supply of the wearable electronic module. We have used it to light up LEDs and power the body temperature module, blood oxygen module, and heart rate module (Figure 5). We combined the power supply module with wearable sensors and placed it on the arm of the subject and collected the data before and after exercise (Figure 5d and video 1). The result showed that, after exercise, blood oxygen levels dropped (Figure 5b), skin surface temperature increased from 30.4 °C to 33.7 °C (Figure 5c), heart rates increased from an average value of 74 beats per minute (b.m.p.) to an average value of 112 b.m.p. (Figure 5e) which also indicated by photoplethysmography (PPG) signals (Figure 5f). The changing trends of these data agree with the changing trends that we recognize. In the following research work, the biofuel cell is expected to power more wearable electronic modules and realize a highly integrated detection and analysis system.

CONCLUSIONS

This paper reports a straightforward strategy to fabricate wearable biofuel cells by the screen-printing method. The biofuel cell consists of a substrate of PDMS screen-printed with conductive MPCs. MPCs are highly conductive (2.7 x 10^5 S/m) to ensure a good electrical performance of the biofuel cells, while their high biocompatibility and stretchability (with a strain of more than 200 %) provide a marked conformability to the bio-interface on human skins. The biofuel cell was used to power wearable sensor (such as a temperature sensor, an oximeter, a heart rate sensor) and monitoring physical index of the subject during exercise. In the future, the biofuel cells may be applied to more stretchable wearable analytical electronics (such as electronic tattoos, epicardial pacing wires, and displays) as green, renewable power supplies.

ASSOCIATED CONTENT

Supporting Information

The Supporting Information is available free of charge at:

Scheme of fabrication of biofuel cells; details of PDMS pellets; SEM images of the MPC and carbon electrodes; the tensile

strain of the MPC; electrochemical performance of anode of the biofuel cell against the concentration of the biofuel; short circuit current of the biofuel cell; the circuit of the energy harvesting module; comparison of MPC and other conductors; the strain of diameter of electrodes (PDF)

The application of the biofuel cell for powering wearable sensors (Video)

AUTHOR INFORMATION

Corresponding Author

Zijian Zheng - School of Fashion and Textiles, Department of Applied Biology and Chemical Technology, Research Institute for Smart Energy, Research Institute for Intelligent Wearable Systems, The Hong Kong Polytechnic University, Hung Hom, Hong Kong S.A.R., China; orcid.org/0000-0002-6653-7594. E-mail: tczzheng@polyu.edu.hk

Xingyu Jiang - Shenzhen Key Laboratory of Smart Healthcare Engineering, Guangdong Provincial Key Laboratory of Advanced Biomaterials, Department of Biomedical Engineering, Southern University of Science and Technology, Shenzhen, Guangdong 518055, China; orcid.org/0000-0002-5008-4703; E-mail: jiang@sustech.edu.cn

Authors

Leni Zhong - Shenzhen Key Laboratory of Smart Healthcare Engineering, Guangdong Provincial Key Laboratory of Advanced Biomaterials, Department of Biomedical Engineering, Southern University of Science and Technology, Shenzhen, Guangdong 518055, China; School of Fashion and Textiles, Department of Applied Biology and Chemical Technology, Research Institute for Smart Energy, Research Institute for Intelligent Wearable Systems, The Hong Kong Polytechnic University, Hung Hom, Hong Kong S.A.R., China; orcid.org/0000-0002-3947-4663.

Lixue Tang - Shenzhen Key Laboratory of Smart Healthcare Engineering, Guangdong Provincial Key Laboratory of Advanced Biomaterials, Department of Biomedical Engineering, Southern University of Science and Technology, Shenzhen, Guangdong 518055, China, orcid.org/0000-0001-9547-1507.

Shuaijian Yang - Shenzhen Key Laboratory of Smart Healthcare Engineering, Guangdong Provincial Key Laboratory of Advanced Biomaterials, Department of Biomedical Engineering, Southern University of Science and Technology, Shenzhen, Guangdong 518055, China, orcid.org/0000-0002-5209-3929

Zhenting Zhao - Shenzhen Key Laboratory of Smart Healthcare Engineering, Guangdong Provincial Key Laboratory of Advanced Biomaterials, Department of Biomedical Engineering, Southern University of Science and Technology, Shenzhen, Guangdong 518055, China, orcid.org/0000-0003-2082-777x.

Author Contributions

Zijian Z. and Xingyu J. supervised this project. Leni Z. and Lixue T. designed and fabricated the BFCs. Leni Z. characterized the device. Zhenting Z. was responsible for circuit design and module construction. Leni Z. and Shuaijian Y. tested wearable sensors and processed the data. All authors discussed the results and wrote the manuscript.

Notes

Any additional relevant notes should be placed here.

ACKNOWLEDGMENT

We thank the National Key R&D Program of China (2021YFF1200800, 2018YFA0902600, 2017YFA0205901,), the National Natural Science Founda-tion of China (21535001, 81730051, 21761142006),the Shenzhen Bay Laboratory (SZBL2019062801004), the Guangdong Innovative and Entrepreneurial Research Team Program (2019ZT08Y191), the Shenzhen Municipal Science and Technology Innovation Council of Shenzhen Government of China (JCYJ20190809151215588, SGDX20190816232209446), the Tencent Foundation through the XPLORER PRIZE for financial support, the Shenzhen Key Lboratory of Smart Healthcare Engineering (ZDSYS20200811144003009), the Guangdong Provincial Key Laboratory of Advanced Biomaterials (2022B1212010003), Dr. Le Wang for fabricating substrates of the biofuel cell, Dr. Qiyao Huang and Dr. Yaokang Zhang for revising the manuscript. We acknowledge the assistance of SUSTech Core Research Facilities.

REFERENCES

(1) Tang, L. X.; Cheng, S. Y.; Zhang, L. Y.; Mi, H. B.; Mou, L.; Yang, S. J.; Huang, Z. W.; Shi, X. H.; Jiang, X. Y. *iScience* **2018**, 4, 302-311.

(2) Dong, R.; Liu, X.; Cheng, S.; Tang, L.; Chen, M.; Zhong, L.; Chen, Z.; Liu, S.; Jiang, X. *Adv. Healthcare Mater.* **2021**, 10, 2000641.

(3) Hang, C.; Ding, L.; Cheng, S.; Dong, R.; Qi, J.; Liu, X.; Liu, Q.; Zhang, Y.; Jiang, X. *Adv. Mater.* **2021**, 33 (36), 2101447.

(4) Mi, H.; Zhong, L.; Tang, X.; Xu, P.; Liu, X.; Luo, T.; Jiang, X. *ACS Appl. Mater. Interfaces* **2021**, 13 (9), 11260-11267.

(5) Cheng, S.; Hang, C.; Ding, L.; Jia, L.; Tang, L.; Mou, L.; Qi, J.; Dong, R.; Zheng, W.; Zhang, Y.; Jiang, X. *Matter* **2020**, 3 (5), 1664-1684.

(6) Ding, L.; Hang, C.; Cheng, S.; Jia, L.; Mou, L.; Tang, L.; Zhang, C.; Xie, Y.; Zheng, W.; Zhang, Y.; Jiang, X. *ACS Nano* **2020**, 14 (12), 16770-16780.

(7) Tang, L.; Mou, L.; Shang, J.; Dou, J.; Zhang, W.; Jiang, X. *Mater. Horizons* **2020**, 7 (4), 1186-1194.

(8) Zhu, M.; Wang, H.; Li, S.; Liang, X.; Zhang, M.; Dai, X.; Zhang, Y. *Adv. Healthcare Mater.* **2021**, 10 (17), 2100646.

(9) Mou, L.; Xia, Y.; Jiang, X. *Anal. Chem.* **2021**, 93 (33), 11525-11531.

(10) Gao, Y.; Guo, Q.; Zhang, Q.; Cui, Y.; Zheng, Z. *Adv. Energy Mater.* **2021**, 11 (15), 2002580.

(11) Gong, X.; Yang, Q.; Zhi, C.; Lee, P. S. *Adv. Energy Mater.* **2021**, 11 (15), 2003308.

(12) Ray, T. R.; Choi, J.; Bandodkar, A. J.; Krishnan, S.; Gutruf, P.; Tian, L.; Ghaffari, R.; Rogers, *J. A. Chem. Rev.* **2019**, 119 (8), 5461-5533.

(13) Zhao, Z.; Huang, Q.; Yan, C.; Liu, Y.; Zeng, X.; Wei, X.; Hu, Y.; Zheng, Z. *Nano Energy* **2020**, 70, 104528.

(14) Ganesh, R. S.; Yoon, H.J.; Kim, S.W. *EcoMat* **2020**, 2 (4), e12065.

(15) Sempionatto, J. R.; Raymundo-Pereira, P. A.; B. Azeredo, N. F.; N. De Loyola e Silva, A.; Angnes, L.; Wang, *J. Chem. Commun.* **2020**, 56 (13), 2004-2007.

(16) Khalid, S.; Raouf, I.; Khan, A.; Kim, N.; Kim, H. S. *Int. J. P.R. Eng. MANGT.* **2019**, 6 (4), 821-851.

(17) Escalona-Villalpando, R. A.; Ortiz-Ortega, E.; Bo-canegra-Ugalde, J. P.; Minteer, S. D.; Ledesma-García, J.; Arriaga, L. G. J. *Power Sources* **2019**, 412, 496-504.

(18) Gai, P.; Song, R.; Zhu, C.; Ji, Y.; Chen, Y.; Zhang, J.R.; Zhu, J.J. *Chem. Commun.* **2015**, 51 (79), 14735-14738.

(19) Chen, Y.; Xianyu, Y.; Wu, J.; Dong, M.; Zheng, W.; Sun, J.; Jiang, X. *Anal. Chem.* **2017**, 89 (10), 5422-5427.

(20) Mou, L.; Zhang, Y.; Feng, Y.; Hong, H.; Xia, Y.; Jiang, X. *Anal. Chem.* **2022**, 94 (5), 2510-2516.

(21) An, S. Y.; Schon, T. B.; McAllister, B. T.; Seferos, D. S. *EcoMat* **2020**, 2 (4), e12055.

(22) Hao, S.; Sun, X.; Zhang, H.; Zhai, J.; Dong, S. J. *Mater. Chem. B* **2020**, 8 (16), 3393-3407.

(23) Fu, Y.; Li, P.; Bu, L.; Wang, T.; Xie, Q.; Chen, J.; Yao, S. *Anal. Chem.* **2011**, 83 (17), 6511-6517.

(24) Jia, W. Z.; Valdes-Ramirez, G.; Bandodkar, A. J.; Windmiller, J. R.; Wang, J. *Angew. Chem. Int. Ed.* **2013**, 52 (28), 7233-7236.

(25) Liu, Y.L.; Jin, Z.H.; Liu, Y.H.; Hu, X.B.; Qin, Y.; Xu, J.Q.; Fan, C.F.; Huang, W.H. *Angew. Chem. Int. Ed.* **2016**, 55 (14), 4537-4541.

(26) Bandodkar, A. J.; You, J.M.; Kim, N.-H.; Gu, Y.; Kumar, R.; Mohan, A. M. V.; Kurniawan, J.; Imani, S.; Nakagawa, T.; Parish, B.; Parthasarathy, M.; Mercier, P. P.; Xu, S.; Wang, J. *Energy Environ.* **2017**, 10 (7), 1581-1589.

(27) Li, P.; Wu, Z.; Hu, H.; Zhang, Y.; Xiao, T.; Lu, X.; Ren, Z.; Li, G.; Wu, Z.; Hao, J.; Zhang, H.L.; Zheng, Z. *ACS Appl. Mater. Interfaces* **2020**, 12 (23), 26050-26059.

(28) Liu, Z.; Zheng, Y.; Jin, L.; Chen, K.; Zhai, H.; Huang, Q.; Chen, Z.; Yi, Y.; Umar, M.; Xu, L.; Li, G.; Song, Q.; Yue, P.; Li, Y.; Zheng, Z. *Adv. Funct. Mater.* **2021**, 31 (14), 2007622.

(29) Yu, Y.; Nassar, J.; Xu, C.; Min, J.; Yang, Y.; Dai, A.; Doshi, R.; Huang, A.; Song, Y.; Gehlhar, R.; Ames, A. D.; Gao, W. *Sci. Robot.* **2020**, 5 (41), eaaz7946.

(30) Liu, Y.L.; Huang, W.H. *Angew. Chem. Int. Ed.* **2021**, 60 (6), 2757-2767.

(31) Chen, X. H.; Yin, L.; Lv, J.; Gross, A. J.; Le, M.; Gutierrez, N. G.; Li, Y.; Jeerapan, I.; Giroud, F.; Berezovska, A.; O'Reilly, R. K.; Xu, S.; Cosnier, S.; Wang, J. *Adv. Funct. Mater.* **2019**, 29 (46).

(32) Greulich, C.; Braun, D.; Peetsch, A.; Diendorf, J.; Siebers, B.; Epple, M.; Köller, M. *RSC Adv.* **2012**, 2 (17), 6981-6987.

(33) Ma, Z.; Huang, Q.; Xu, Q.; Zhuang, Q.; Zhao, X.; Yang, Y.; Qiu, H.; Yang, Z.; Wang, C.; Chai, Y.; Zheng, Z. *Nat. Mater.* **2021**, 20 (6), 859-868.

(34) Tang, L.; Mou, L.; Zhang, W.; Jiang, X. *ACS Appl. Mater. Interfaces* **2019**, 11 (7), 7138-7147.

(35) Tang, L.; Shang, J.; Jiang, X. *Sci. Adv.* **2021**, 7 (3), eabe3778.

(36) Wu, S.M.; Jiang, N.; Hu, Z.Y.; Yan, T.; Jin, J.; Geng, W.; Yang, X.Y. *Chem. Phys. Lett.* **2019**, 717, 29-33.

(37) Wang, L.; Li, Y.; Yang, X.Y.; Zhang, B.-B.; Ninane, N.; Busscher, H. J.; Hu, Z.Y.; Delneuville, C.; Jiang, N.; Xie, H.; Van Tendeloo, G.; Hasan, T.; Su, B.L. *Natl. Sci. Rev.* **2020**, 8 (4), nwaa097.

(38) Niu, J.; Lunn, D. J.; Pusuluri, A.; Yoo, J. I.; O'Malley, M. A.; Mitragotri, S.; Soh, H. T.; Hawker, C. J. *Nat. Chem.* **2017**, 9 (6), 537-545.

(39) Ashok Kumar, N.; Baek, J.B. *Chem. Commun.* **2014**, 50 (48), 6298-6308.

(40) Xia, L.; Xia, J.; Wang, Z. *RSC Adv.* **2015**, 5 (113), 93209-93214.

(41) Geng, W.; Wang, L.; Jiang, N.; Cao, J.; Xiao, Y.X.; Wei, H.; Yetisen, A. K.; Yang, X.Y.; Su, B.L. *Nanoscale* **2018**, 10 (7), 3112-3129.

(42) Tsujimura, S. *Biosci. Biotechnol. Biochem.* **2019**, 83 (1), 39-48.

Liquid-metal-based metal-polymer conductors are employed as electrodes for stretchable and wearable biofuel cells (BFCs), which accommodate the motions of human skins and generate energy from sweat.